Orthorhombic (Fe$_2$TiO$_5$)-monoclinic (Cr$_2$TiO$_5$) solid solution series: Synthesis by gel routes, coloring and NIR reflectivity evaluation

S. Cerro, C. Gargori, M. Llusar, G. Monrós*

Dpt. of Inorganic and Organic Chemistry, Jaume I University, Av. de Vicent Sos Baynat, s/n., 12071 Castellón, Spain

ARTICLE INFO

ABSTRACT

Cr$_x$Fe$_{2-x}$TiO$_5$ compositions of the solid solutions series from pseudobrookite Fe$_2$TiO$_5$ to monoclinic Cr$_2$TiO$_5$ have been prepared by the ceramic route and gel methods. At 1400 °C, pseudobrookite crystallizes in the x = 0–0.4 range, both pseudobrookite and monoclinic Fe-Cr$_2$TiO$_5$ coexist at x = 0.5, while in the range x = 0.7–1.5 monoclinic Fe-Cr$_2$TiO$_5$ crystallizes. Powders were 5 wt% glazed within a double-firing frit and the composition with x = 0.1 fired at 1000 °C exhibits the best red color (L*a*b* = 43.2/18.8/12.5), showing an intense band at 520 nm in the UV–Vis–NIR absorption spectrum associated with Cr^{4+} in octahedral coordination. The unit cell volume of the pseudobrookite decreases smoothly with the chromium amount, associated with the entrance of Cr^{4+} replacing Ti^{4+}, while the volume of the Fe-Cr$_2$TiO$_5$ unit cell increases with the entrance of Fe^{3+} replacing Cr^{3+}. The use of flux agents, the compaction pressure and the gel methods increase the crystallization of pseudobrookite but do not improve the reddish color, which is associated with the concentration of Cr^{4+} in the pigment. The optimized pigment composition Cr$_{0.1}$Fe$_{1.9}$TiO$_5$ also shows a high NIR reflectance (55% in powder, 54% in glazed sample).

1. Introduction

Pseudobrookite Fe$_2$TiO$_5$ is a reddish brown to ochre-yellow colored mineral that was first described by Pauling [1] in 1930. The structure of pseudobrookite (general formula AB$_2$O$_5$) shows orthorhombic symmetry (*Cmcm* space group) and gives its name to a large group of isostructural phases. The group of Ti pseudobrookites, including FeTi$_2$O$_5$, MgTi$_2$O$_5$, Fe$_2$TiO$_5$, Al$_2$TiO$_5$, Ga$_2$TiO$_5$ and Ti$_3$O$_5$, have an extraordinary structure flexibility to accommodate many distinct metals (with +2, +3 or +4 oxidation states) in their two different and distorted octahedral cationic sites, A (4c) and B (8 f), giving rise to a number of solid solutions with general formula [M^{3+},M^{2+},Ti]^A [Ti,M^{2+},M^{3+}]$^B_2$O$_5$. This property, along with their high melting point and high refractive index (2.4 for Fe$_2$TiO$_5$) [2], allow Ti pseudobrookites to be excellent candidates for the development of new pigments. Indeed, some patents about yellow pigments based on Ti pseudobrookites have been already developed (Rademachers [3], Maloney [4], Katamoto [5] and Suzuki [6]), basically for low-temperature applications (paints, plastics, resins, etc.). Moreover, some recent studies show that Ti pseudobrookites may also be used as ceramic pigments for the coloration of glazes under more severe firing treatments [7–10].

Pseudobrookites are entropy-stabilized phases [11,12], that is to say, the cationic disorder contributes the entropic component to stabilize pseudobrookite phase at high temperatures. By decreasing the temperature, pseudobrookites decompose in the thermodynamically most stable phases, either a mixture of binary oxides M$_2$O$_3$ and TiO$_2$ (pseudobrookites M$_2^{3+}$Ti^{4+}O$_5$), a mixture of ilmenite MTiO$_3$ and rutile TiO$_2$ (pseudobrookites M^{2+}Ti$_2^{4+}$O$_5$) [12], or giving rise to a smaller symmetry phase (Ti$_3$O$_5$ case) [13]. In this regard, the higher or lower thermal stability of pseudobrookites is strongly dependent on its composition; this decomposition can be inhibited obtaining stabilized pseudobrookite at low temperatures or even at room temperature by adding different dopants or forming solid solutions.

The solid solution from Fe$_2$TiO$_5$ to FeTi$_2$O$_5$ was studied by Gray and Ward [14] and also by Navrotsky [15]. It has commonly been observed that naturally occurring minerals with pseudobrookite structure have intermediate compositions; thus, in addition to varying proportions of Fe^{2+} and Fe^{3+} [16], other ions such as Mg^{2+}, Mn^{2+}/Mn^{3+}, Al^{3+}, and Cr^{3+}/ Cr^{4+} frequently occur. It is well known that for the synthesis of iron pseudobrookite Fe$_2$TiO$_5$ from anatase an iron (III) oxide, a significant excess of titania with respect to the Fe$_2$TiO$_5$ stoichiometry is needed, in order to "achieve a complete reaction of the iron oxide" and to obtain a hematite-free pseudobrookite [17]. In effect, Seitz et al. [18] conclude from Rietveld analyses that the stoichiometry of hematite-free pseudobrookite is Fe$_{1.94}$Ti$_{1.06}$O$_5$ at 900 °C and Fe$_{1.91}$Ti$_{1.09}$O$_5$ at 1400 °C. Furthermore, the pseudobrookite phase obtained by sintering under air

atmosphere does not have the Fe_2TiO_5 stoichiometric composition (it shows iron/titanium ratio lower than 2) and, moreover, this composition varies with the temperature of thermal treatment. Seitz et al. propose two hypotheses to explain this variation of stoichiometric composition: (i) the thermal treatment under air leads to an average oxidation number intermediate between 2 and 3 for the iron ions, and (ii) the occurrence of cation vacancies, concomitantly to a dense anionic subnetwork. However, the Mössbauer study performed on samples constituted by a single pseudobrookite phase strongly suggests that crystallization of a pure pseudobrookite phase from iron-deficient chemical compositions (iron/titanium < 2) is not due to stabilization of Fe^{2+} into the bulk but to the occurrence of cation vacancies [18]: a proposed formulation can be written as $(Fe_{2-x}^{3+}Ti_{1+x}^{4+})_{1-z}V_zO_5$, with the electroneutrality of the composition leading to the vacancy concentration $z = x/(x + 10)$; for instance, $z \sim 0.006$ ($x \sim 0.06$) and $z \sim 0.009$ ($x \sim 0.09$) for the hematite-free pseudobrookite at 900 and 1400 °C respectively.

Yellow-ochre to reddish maroon or brown hues can be obtained by substituting iron or titanium ions with other metallic cations in pseudobrookite (e.g., Mg^{2+}). Pseudobrookite-based pigments were first developed in the 1970s in order to get heat-resistant colorants for thermoplastics, industrial paints, and other applications involving low-temperature treatments [18]. Dondi et al. [8] have studied the potentialities of these types of compounds for ceramic pigment applications, i.e., applications involving high-temperature treatment. The colors achievable with pseudobrookite pigments are significantly dependent on the composition of ceramic matrices, varying from saturated brown shades achieved in low temperature glasses to a lighter brown in stoneware glazes, while the colors fade to a light gray in highly opacified glazes for wall tiles, where the high CaO and ZnO content contributes to rapid dissolution of the pigment [8]. According to Dondi et al., the color is originated by several light absorptions in the visible spectrum due to both d^5 electrons transitions and a magnetically-coupled paired transition between iron ions in adjacent lattice sites. A doubling of the $^6A_1 \rightarrow ^4T_1$ and $^4T_2$ bands is related to the occurrence of Fe^{3+} in both octahedral sites of pseudobrookite [5]. Recently, Gargori et al. [19] described a red-brown ceramic pigment based on chromium-doped ferrian armalcolite $(MgFe)(FeTi_3)O_{10}$, which belongs to the pseudobrookite group X_2YO_5, with X and Y being usually Fe (2 + and 3 +), Mg, Al, and Ti. End members of this group are armalcolite $((Mg,Fe)Ti_2O_5)$, pseudobrookite (Fe_2TiO_5), ferropseudobrookite $(FeTi_2O_5)$ and karrooite $(MgTi_2O_5)$.

The compound Cr_2TiO_5 could be synthesized as a stoichiometric single phase above 1660 °C in air [20]. Application of selected area electron diffraction, high resolution electron microscopy and powder X-ray diffraction studies showed that Cr_2TiO_5 is isomorphic with $CrFeTiO_5$, which shows V_3O_5 oxyvanite monoclinic type structure (space group *C2/c*), showing cell parameters a = 7.020(1)Å, b = 5.025(1)Å, c = 9.945(2)Å and β = 111.43(2)° (JCPDS 73-0409). It was found that Cr_2TiO_5 is unstable relative to a mixture of Cr_2O_3 (ss) and a so-called "E" phase below 1660 °C [20].

In the literature there is a controversy about the existence of a monoclinic polymorph for Fe_2TiO_5 orthorhombic pseudobrookite. Shiojiri et al. [21] reported a doubtful new monoclinic structure for Fe_2TiO_5. The crystal structure of metal pseudobrookite (Fe_2TiO_5) is determined by Shiojiri et al. from high-resolution electron microscopy images and their computer simulated images, with the aid of electron diffraction and X-ray powder diffraction. The new structure would have a monoclinic unit, containing eight molecules, with a = 2.223, b = 0.373, c = 0.980 nm, and β = 116.2° [22]. Other authors detect a monoclinic Fe_2TiO_5 (JCPDS 73-1898, having lattice parameters a = 10.101, b = 5.037, c = 7.024 Å) with XRD peaks associated with nanostructured materials, which show a wide profile and relatively low intensity of peaks due to the low particle size of the involved nanoparticles [22,23]. A monoclinic form of Fe_2TiO_5, metastable in nature, has been artificially grown as single crystals from a flux containing

various amounts of the basic oxides and characterized by Mössbauer spectroscopy [24], but the occurrence of this controverted polymorph from a solid state reaction is unusual. The most comprehensive work on orthorhombic Fe_2TiO_5 and its solid solution with $FeTi_2O_5$ is the paper of Guo et al. [25], which shows that the whole solid-solution series has the pseudobrookite (*Cmcm*) structure type. Guo et al. emphasize that no diffraction peaks associated to monoclinic specimen were detected in any of the samples prepared for their study. Therefore Guo et al. found no evidence for the monoclinic phase reported by Shiojiri et al. [21].

The monoclinic Cr_2TiO_5, unstable at room temperature, is isostructural with V_3O_5-type gamma-Ti_3O_5, $CrFeTiO_5$ and V_2TiO_5 [26]. In this communication chromium-doped pseudobrookite compositions of the $Cr_xFe_{2-x}TiO_5$ solid solutions series from pseudobrookite Fe_2TiO_5 (x = 0) to Cr_2TiO_5 (x = 2) have been studied in order to stabilize a red-brown pigment in CaO-ZnO-SiO_2 ceramic matrices. The effect of several flux agents as mineralizers and the use of non-conventional synthesis methods such as ammonia coprecipitation (CO), citrate route or metal-organic decomposition method (MOD) and a polymeric gel (GP) method have also been studied.

On the other hand, the synthesis of pigments showing high NIR reflectance (the so-called "cool pigments") is highly demanded nowadays, since they can help reduce the temperature of the external walls and therefore the temperature inside of buildings, thus reducing the power consumption during hot weather. Therefore, the NIR reflectance of an optimized $Cr_xFe_{2-x}TiO_5$ composition is compared with a commercially available (Zn-Fe-Cr) brown spinel (CPMA 13-37-7) [27] in order to evaluate the pigment suitability as an energy-saving material.

2. Materials and methods

2.1. Samples preparation

$Cr_xFe_{2-x}TiO_5$ compositions have been prepared by the ceramic route (or solid state reaction method), using as precursors Fe_2O_3 and TiO_2 (anatase) supplied by Panreac S.A., and Cr_2O_3 supplied by Riëdel. In this ceramic method the precursors were homogenized in a planetary mill in acetone media. Once acetone was evaporated the raw powders were fired successively at 1000, 1200 and 1400 °C with a soaking time of 3 h and with free cooling to room temperature. The as-prepared powders were homogenized manually with mortar and pestle, and the resulting powders were 5 wt% glazed into a conventional double-firing frit of the CaO-ZnO-SiO_2 system (1050 °C) in order to characterize its pigmenting properties.

The effect of the presence of flux agents on the reactivity of the system was studied by addition of several mineralizers (10 wt%) to the ceramic mixture x = 0.1 and fired successively at 1000 and 1100 °C with soaking times of 3 h. The tested mineralizers were: a) two low temperature mineralizers such as H_3BO_3 (melting point m.p. 170.9 °C) and NH_4Cl (decomposes at 338 °C), b) a middle temperature mineralizer Li_2CO_3 (m.p.723 °C), and c) a relatively high temperature flux agent NaF (m.p. 993 °C). On the other hand, x = 0.1 samples (both non-mineralized and mineralized with NH_4Cl) were pelleted at 100 bar in a conventional press and fired at 1000 °C for 2 h, in order to study the effect of powder compaction on the reactivity and color of the pigment.

Moreover, the effect of three non-conventional methods of preparation based on gel techniques was also studied for the optimized x = 0.1 composition. In the coprecipitation or colloidal-gel method (CO), $Cr(NO_3)_3 \cdot 6H_2O$, $Fe(NO_3)_3 \cdot 6H_2O$ and titanium(IV) n-butoxide (for 10 g of $Cr_{.1}Fe_{1.9}TiO_5$ final product and all supplied by ALDRICH S.A.) were successively dissolved at room temperature and continuously stirred in 200 mL of water, then ammonia solution (15 wt%) were dropped to the stirred solution until pH = 8 is reached; finally, the obtained gel was dried at 110 °C. In the MOD (metal-organic decomposition) or citrate-gel method, the same precursors of CO method (for 10 g of $Cr_{.1}Fe_{1.9}TiO_5$ final product) were successively dissolved at room temperature and continuously stirred in 200 mL of water. Then citric

acid, in a molar ratio citric acid: pseudobrookite = 1:2, was added to the stirred solution and the obtained solution was also dried at 110 °C. Finally in the GP (polymeric gel) method, the same precursors of CO route (for 10 g of $Cr_{.1}Fe_{1.9}TiO_5$ final product) were successively dissolved at room temperature and continuously stirred in 200 mL of ethanol. The solution was closed to the air by a polyethylene film and maintained for 24 h at room temperature with continuous stirring in order to promote the hydrolysis-polymerization of the mixture; then, the obtained gel was dried at 110 °C. All dried gels were fired at 500 °C for 1 h (charring procedure) for its stabilization, and then they were calcined at 1000 °C for 3 h along with the CE sample.

2.2. Samples characterization

X-Ray Diffraction (XRD) was carried out on a Siemens D5000 diffractometer using Cu K_α radiation, 10–70° 2θ range, scan rate 0.02°2θ/ s, 4s per step and 40 kV and 20 mA conditions. In order to measure the parameters of the crystalline unit cell through POWCAL and LSQC programs [28], α-Al_2O_3 was added (40 wt%) as internal standard, and XRD patterns were recorded at 20–70°2θ range under slower conditions (scan rate 0.01°2θ/s, 10 s per step and 40 kV and 20 mA).

UV–Vis–NIR spectra of fired powder samples and also of 5 wt% glazed samples (in a conventional double-firing frit on the SiO_2-CaO-ZnO system (1050 °C)) were collected using a Jasco V670 spectrometer through diffuse reflectance technique which gives data in absorbance using arbitrary units (A), or in reflectance units (R(%)) using the Kubelka-Munk transformation model. The Kubelka-Munk (K-M) function model has a particularly simple solution in the case of reflection of radiant energy at boundary surfaces of mat (dull, scattering) surfaces [29,30]. L*a*b* color parameters of glazed samples were measured following the CIE-L*a*b* (Commission Internationale de l'Éclairage) colorimetric method [31] using a X-Rite SP60 spectrometer, with standard lighting D65 and 10° observer. On this method, L* is a measure of lightness (100 = white, 0 = black) and a* and b* of chroma (-a* = green, +a* = red, -b* = blue, +b* = yellow). The optical reflectance spectrum was scanned in the range of 300–2500 nm for the optimized pigment, and the total solar reflectance (R) and the NIR solar reflectance (R_{NIR}) were obtained as the integral of the measured spectral reflectance and the solar irradiance divided by the integral of the solar irradiance in the range of 350–2500 nm for R or 750–2500 nm for R_{NIR}, as in the Eq. (1):

$$R = \frac{\int_{350}^{2500} r(\lambda) i(\lambda) d\lambda}{\int_{350}^{2500} i(\lambda) d\lambda} \qquad (1)$$

where, $r(\lambda)$ is the spectral reflectance $(W\,m^{-2})$ measured from UV–Vis–NIR spectroscopy and $i(\lambda)$ is the standard solar irradiation $(W\,m^{-2}\,nm^{-1})$ according to the American Society for Testing and Materials (ASTM) Standard G173-03 [32].

Microstructure characterization of powders was carried out by Scanning Electron Microscopy (SEM) using a JEOL 7001 F electron microscope (following conventional preparation and imaging techniques). The chemical composition and homogeneity of the samples was determined by semi-quantitative elemental analysis with an EDX analyzer (supplied by Oxford University) attached to the microscope.

3. Results and discussion

3.1. X-Ray diffraction characterization (XRD)

XRD results obtained with fired powders are summarized in Table 1 and the corresponding XRD patterns of samples fired at 1400 °C are shown in Fig. 1. All fired samples are red-brown colored and its XRD patterns indicate the following evolution of crystalline phases:

a) At 1000 °C, hematite peaks predominate in the XRD pattern of

Table 1
XRD evolution with temperature of $(Fe_{2-x}Cr_x)TiO_5$ samples. CRYSTALLINE PHASES: P (Cr-Fe_2TiO_5 orthorhombic), M (Fe-Cr_2TiO_5 monoclinic), H (Hematite Fe_2O_3), C (Eskolaite Cr_2O_3, E ($Cr_2Ti_2O_7$ phase "E"[20,31]), R (Rutile), I (unidentified). PEAK INTENSITY vs(very strong), s(strong), m(medium), w(weak), vw(very weak).

Sample	1000 °C	1200 °C	1400 °C
x = 0	P(m)H(s)R(m)	P(vs)H(vw)	P(vs)H(vw)
x = 0.1	P(s)H(s)R(m)	P(vs) H(vw)	P(vs)H(vw)
x = 0.3	P(s)H(m)R(w)	P(vs) H(vw)	P(vs)H(vw)
x = 0.5	M,H(m)	M(m)P,H(w)	P,M(s)H(vw)
x = 0.7	M,H(m)	M(m)H(vw)	M(s)
x = 1	C(s)M,R(m)	M(s)C(vw)	M(s)
x = 1.5	C(s)M,R(m)	M(s)C(vw)	M(s)
x = 2	C(s)R(m)	C(s)R(m)	C,E,I(m)

sample with x = 0 (undoped pseudobrookite), samples with x = 0.1 and x = 0.3 show orthorhombic pseudobrookite as the main phase, that turns into monoclinic Fe-Cr_2TiO_5 in x = 0.5 and x = 0.7 samples. Samples with higher x values show predominant diffraction peaks associated with the reactants eskolaite (Cr_2O_3) and rutile (TiO_2).

b) At 1200 °C, samples with x = 0 to x = 0.3 show strong diffraction peaks associated with orthorhombic pseudobrookite and weak peaks of residual hematite; at higher x values the monoclinic Fe-Cr_2TiO_5 predominates, but sample x = 2 still remains unreacted, since only the peaks associated with the reactants are detected.

c) At 1400 °C, samples up to x = 0.5 show pseudobrookite as predominant crystalline phase, but some residual hematite is also detected; at x = 0.5 both pseudobrookite and monoclinic Fe-Cr_2TiO_5 coexist, while at higher x values monoclinic Fe-Cr_2TiO_5 is detected. However, in sample x = 2 the peaks of monoclinic Cr_2TiO_5 are not detected and, instead, the XRD pattern shows the presence of a mixture of Cr_2O_3 (ss), $Cr_2Ti_2O_7$ (the so-called "E" phase) [20], along with other unidentified peaks (Fig. 1). These peaks could probably be associated with the discrete homologous series of $Cr_2Ti_{n-2}O_{2n-1}$ (with n = 6, 7, 8) that were found to be stable as single phases in certain temperatures range, in agreement with S. Sōmiya et al. [33].

The described evolution of the crystalline phases agrees with previous reports: for instance, Seitz et al. [18] postulate the presence of cation vacancies that lead to a proposed formulation written as $(Fe_{2-x}^{3+}Ti_{1+x}^{4+})_{1-z}V_zO_5$, in order to explain that the pseudobrookite phase obtained under air conditions does not show the Fe_2TiO_5 stoichiometric composition and the fact that this composition varies with firing temperature. In effect, in the case of samples between x = 0 and x = 0.5, hematite always appears as residual phase along with pseudobrookite, which cannot be obtained as the single crystalline phase. In contrast, monoclinic Fe-Cr_2TiO_5 is obtained as single phase in samples between x = 0.7 to x = 1.5 (Fig. 1).

3.2. Color evolution of samples

CIE-L*a*b* color measurements of fired powders and of 5 wt% glazed samples into a CaO–ZnO–SiO2 conventional glaze are shown in Table 2. The results indicate that the progressive introduction of chromium decreases L* parameter (samples become darker) and also decreases both a* and b* parameters of the powders, in agreement with the visual perception. Likewise, when the firing temperature increases, the color evolution is similar and samples become darker and more bluish (all L*, a* and b* parameters decrease).

When the powders are 5 wt% glazed in a double-firing frit (1050 °C) the non-doped chromium sample becomes practically colorless: at 1000 °C this sample shows a very light yellowish color (L*a*b* = 71.8/ 2.6/22.8, see Table 2), and also at 1400 °C (L*a*b* = 71.3/1.1/9.5, see
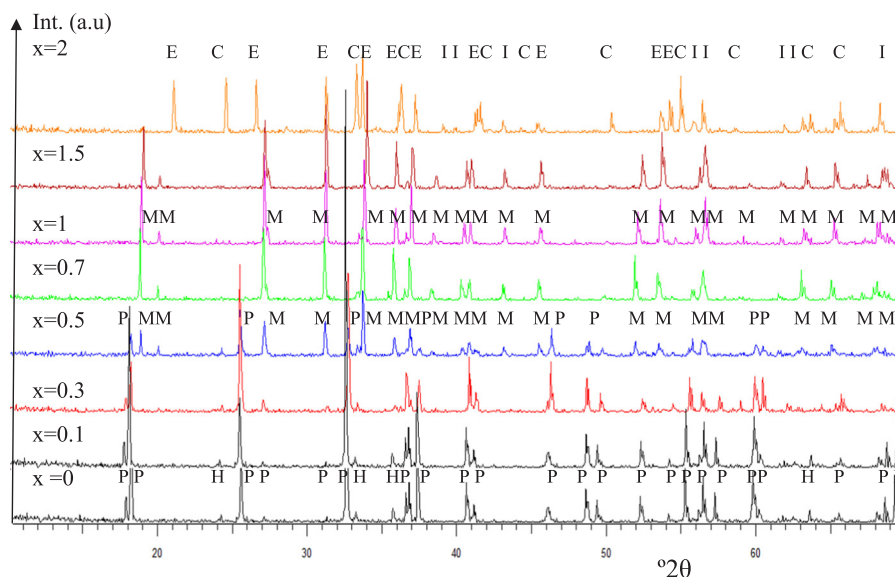
Fig. 1. XRD of $(Fe_{2-x}Cr_x)TiO_5$ samples fired at 1400 °C/3 h CRYSTALLINE PHASES: P (Cr-Fe_2TiO_5 orthorhombic), M (Fe-Cr_2TiO_5 monoclinic), H (Hematite Fe_2O_3), C (Eskolaite Cr_2O_3) I (unidentified).

Table 2 and Fig. 2), associated with a L* value higher than 71. This result indicates that chromium is the responsible for the brown shade of the glaze. In these glazed samples, the best red-brown color is obtained at 1000 °C: the x = 0.1 sample with L*a*b* = 43.2/18.8/12.5 shows the highest red chroma (positive a* value) of the prepared samples, showing a relatively high intensity of color (low L*). As a reference or comparison, a commercial pink coral based on hematite inclusion into zircon crystals shows L*a*b* = 53/26/24, namely, higher a* red shade and lower intensity than the optimized sample x = 0.1, while the commercially available brown pigment based on Zn-Fe-Cr spinel (CPMA 13-37-7) [27] shows L*a*b* = 32.6/13.0/9.2, with higher intensity of color but lower a* red parameter; finally, the best red-brown hue obtained with the closely related chromium doped ferrian armalcolite (MgFe)$(Cr_{0,2}Ti_{2,8}Fe)O_{10}$ obtained at 1000 °C shows L*a*b* = 49.5/15.2/10.3, with both lower intensity L* and lower a* red parameter [19].

On the other hand, as the firing temperature of powders increases (Table 2), a strong decrease of both L* and red a* parameters is detected. Likewise, the b* parameter turns into a blue shade (negative values) and the powders are black colored.

Similar evolution is observed in glazed samples (see Table 2):

a) At 1000 °C, associated to the lowest reactivity of the system (lowest crystallization of pseudobrookite or monoclinic Fe-Cr_2TiO_5): the reddish shade (evaluated by a*) is the best, varying from 12.0 (x = 1.5) to 18.8 (x = 0.1).

b) At 1200 °C, associated with large crystallization of pseudobrookite or monoclinic Fe-Cr_2TiO_5 phases: the intensity of the color decreases

(higher L*) and the red shade also decreases to 8.8 (x = 1.5) and 12.2 (x = 0.1) respectively.

c) When the reactivity is completed at 1400 °C: the intensity continues to fall and the reddish value a* also decreases to 6.4–7.6.

From the above discussed XRD and CIEL*a*b* results, it can be pointed out that the red-brown color of glazed samples is associated with the presence of chromium (since the glaze becomes colorless without Cr (x = 0)), and it becomes green in sample x = 2 (showing eskolaite Cr_2O_3 and the E phase, $Cr_2Ti_2O_7$, as detected phases) (Fig. 2). However, the best red-brown colors are not associated with a complete crystallization of pseudobrookite or monoclinic Cr_2TiO_5 phase; indeed, when its crystallization progresses with temperature, powders become practically black colored and glazed samples show low reddish shades (high values of L* and low values of both a* and b*).

3.3. UV–Vis–NIR absorption spectra

The UV–Vis–NIR absorption spectra of fired powders are shown in Fig. 3. The following bands are detected: (a) intense bands at 200–300 nm, (b) intense band centered at 400 nm overlapping with (a), (c) strong shoulder at 510 nm, (d) weak shoulder at 600 nm, (e) weak band at 700 nm, and (f) a very weak band at 900 nm. It is difficult to distinguish the presence of Cr^{3+}, Cr^{4+} or Fe^{3+} ions in octahedral sites in UV–Vis–NIR absorption spectra of samples containing the ions in these positions simultaneously [34–36], because the bands of Cr^{3+} and Cr^{4+} are overlapped to a high extent with the absorption bands of iron (III). But the main characteristic of the Fe^{3+} ions in octahedral sites is

Table 2
CIEL*a*b* evolution with temperature of $(Fe_{2-x}Cr_x)TiO_5$ of powder and glazed samples: *(L*a*b*) values separated by bars.

Sample	1000 °C		1200 °C		1400 °C	
	Powder	Glazed	Powder	Glazed	Powder	Glazed
x = 0	48.0/8.9/12.1 *	71.8/2.6/22.8	43.0/8.2/7.7	72.3/0.1/13.5	40.0/7.7/7.7	71.3/1.1/9.5
x = 0.1	46.2/6.8/7.6	**43.2/18.8/12.5**	41.6/4.4/2.3	50.3/12.2/9.2	39.6/3.7/2.3	54.0/6.6/2.8
x = 0.3	46.0/6.0/5.6	42.9/17.0/12.1	41.1/3.6/1.3	47.3/11.2/7.2	39.0/3.1/2.0	48.6/7.6/2.5
x = 0.5	40.8/3.1/1.8	42.2/15.0/12.6	40.8/2.8/− 0.4	46.2/10.7/6.9	38.7/2.8/2.0	46.8/7.5/4.7
x = 0.7	40.1/2.9/1.9	41.8/14.7/12.2	40.2/2.9/− 0.3	45.2/10.1/5.9	38.8/2.5/1.7	45.6/6.8/4.3
x = 1	39.8/2.9/2,7	41.2/16.1/15.6	39.6/2.8/− 0.2	44.4/9.3/5.1	38.2/2.0/0.8	45.2/6.7/4.8
x = 1.5	38.3/2.0/1.5	40.0/12.0/1.2	38.0/1.6/− 0.5	43.4/8.8/4.1	37.8/1,1/− 0.2	44.1/6.4/2.2
x = 2	41.7/− 12.7/16.1	49.3/− 13.5/13	40.6/− 11.7/12.1	48.8/− 9.5/9.1	40.0/− 9.7/8.1	48.9/− 8.4/4.3
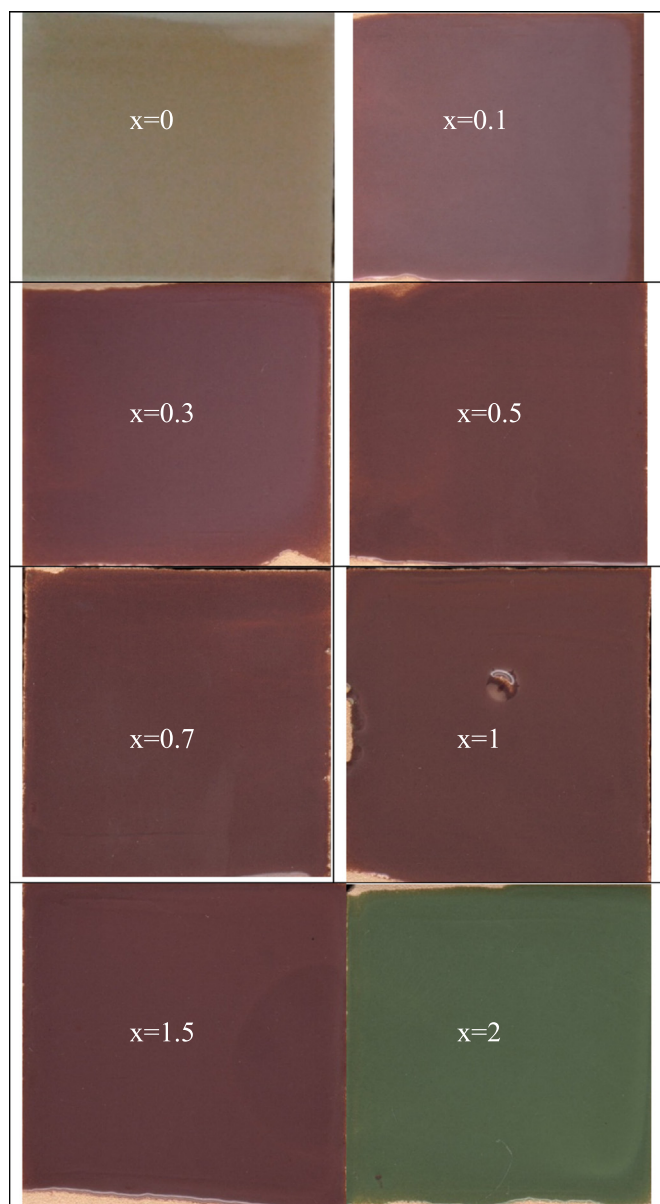
Fig. 2. Photographs of glazed samples of powders fired at 1400 °C.

Fig. 3. UV–Vis–NIR absorbance spectra of powders x = 0.1, 0.5 and 1.0: a) fired at 1000 °C, b) at 1200 °C: A(a.u.) is the absorbance in arbitrary units.

Fig. 4. UV–Vis–NIR absorbance spectra of glazed sample x = 0 at 1000 °C and 1200 °C.

the strong absorption associated to the transitions $^6A_{1g}(S) \rightarrow {}^4A_{1g}, {}^4E(G)$ at 450 nm and $^6A_{1g}(S) \rightarrow {}^4T_{2g}(D)$ at 400 nm that dominates the absorption spectrum of the powders either at 1000 °C or 1200 °C (Fig. 3) [19].

UV–Vis–NIR absorption spectra of non-doped (without chromium) glazed samples are shown in Fig. 4; according to the colorless shade of the samples, only an intense absorption band due to the charge transfer associated to the glaze centered at 280 nm has been detected, along with a very weak band centered at 450 nm associated with Fe^{3+} ions in octahedral sites. The UV–Vis–NIR absorption spectra of Cr-doped glazed samples are shown in Fig. 5 and the detected bands are the following: (a) intense band at 270 nm due to the charge transfer of the glassy matrix of the glazed samples, (b) intense band centered at 520 nm, (c) weak shoulder at 600 nm, (d) double weak bands at 700 nm, (e) weak shoulder at 850 nm, and (f) a very weak band at 900 nm. The strong absorption in the range 400–450 nm has disappeared and, along with the intense ion charge transfer of the bulk glaze, an intense band at 520 nm dominates the spectrum, indicating the presence of Cr^{4+} in octahedral coordination with its characteristic absorption band centered at 520 nm [19,37,38]. On the other hand, the
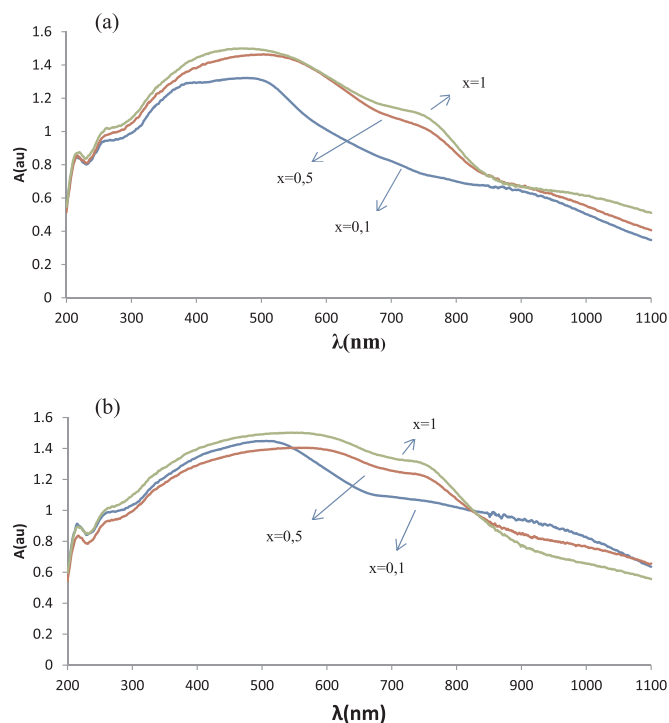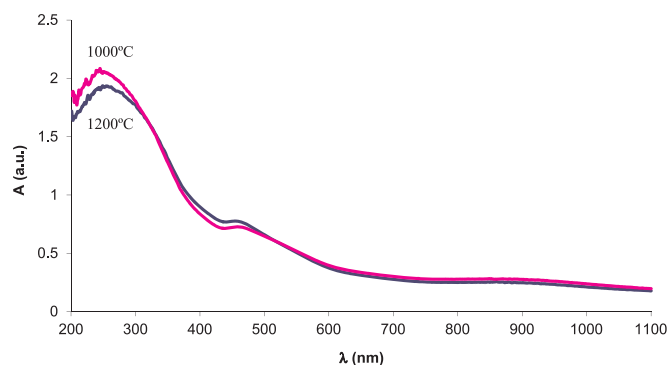
intensity (optical density) of absorption bands in the spectra of glazed samples increases when the amount of chromium increases from x = 0 to x = 0.5 (pseudobrookite crystallization field, Fig. 5.a) and decreases from x = 0.5 to x = 1.5 (monoclinic Fe-Cr₂TiO₅ crystallization field, Fig. 5.b). Finally, the weak shoulder at 600 nm and the double weak band at 700 nm, both of them detected more evidently when chromium amount increases in the pseudobrookite crystallization field (from x = 0 to x = 0.5), indicate a progressive presence of Cr^{3+} in octahedral sites in agreement with literature [19,39,40]. On the other hand, the optical density of these Cr^{3+} bands decreases with x in the monoclinic Fe-Cr₂TiO₅ crystallization field (from x = 0.5 to x = 1.5), but the 520 nm band intensity associated to Cr^{4+} in octahedral sites remains stable, indicating a saturation of Cr^{4+} concentration at around x = 0.5. These results are in agreement with the evolution of the reddish a* parameter of glazed samples in Table 2: a* increases slightly from x = 0.1 to x = 0.7 samples, associated with the increase of optical density at 520 nm due to Cr^{4+}, and remains practically stable in the monoclinic Fe-Cr₂TiO₅ crystallization field (from x = 0.7 to x = 1.5, with values around a* = 6.7), associated with a stable optical density of the 520 nm band of Cr^{4+} in these samples.
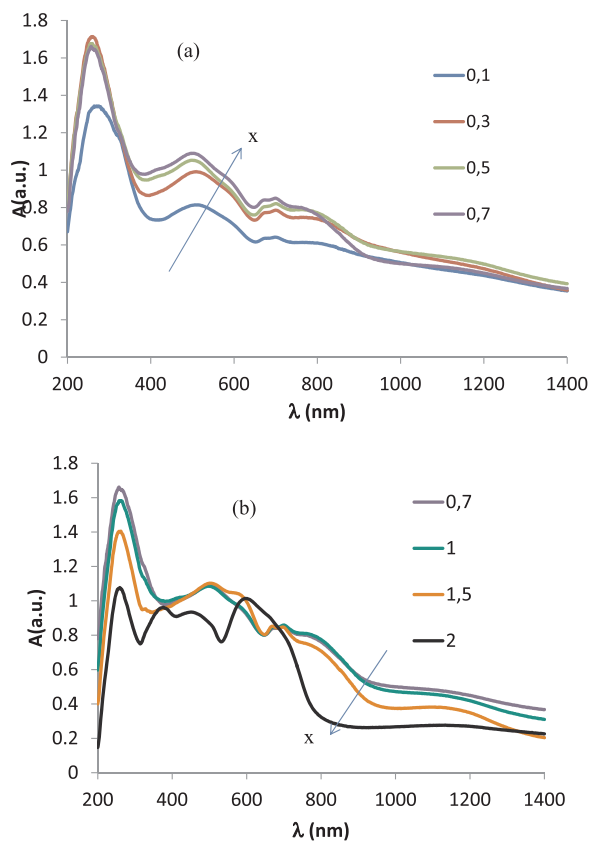
Fig. 5. UV–Vis–NIR absorbance spectra of glazed samples at 1400 °C: (a) x = 0.1–0.7, (b) x = 0.7–2.

Fig. 6. Unit cell parameters evolution with chromium content in samples fired at 1400 °C.

Thereby, although the assignment of bands is difficult because of the overlapping of the absorptions of Cr^{3+}, Cr^{4+} and Fe^{3+} ions in octahedral coordination, the analysis of the UV–Vis–NIR absorption spectra shows that chromium is the chromophore in the glazes, predominating the oxidation state + 4, although Cr^{3+} concentration increases when chromium amount increases. This behavior is in agreement with the color and the evolution of the CIEL*a*b* values of glazed samples: the intensity of the color increases always with both chromium amount and temperature (L* diminishes) and the red-brown chroma tends to blue, due to the enhancement of the 600 nm (orange) absorption band when chromium amount or temperature increase.

3.4. Evolution of crystalline unit cell parameters with the amount of chromium

Unit cell parameters were measured in powders fired at 1400 °C (Table 3). The evolution of the volume of the crystalline unit cell with chromium amount (x) is shown in Fig. 6 and the following

characteristics can be pointed out:

a) From x = 0 up to x = 0.5, in which the presence of Fe_2TiO_5 pseudobrookite dominates or coexists (x = 0.5) with $Fe-Cr_2TiO_5$ monoclinic phase, the volume of the pseudobrookite unit cell decreases smoothly with the chromium amount according to the entrance of Cr^{4+} (Shannon-Prewitt ionic radius 0.69 Å in coordination VI) in the structure of the pseudobrookite, replacing Ti^{4+} (0.745 Å in coordination VI) [41].

b) From x = 0.5 to x = 1.5, in which the $Fe-Cr_2TiO_5$ monoclinic phase coexists with Fe_2TiO_5 pseudobrookite (at x = 0.5) or dominates the system, the unit cell decreases smoothly with the chromium amount. Indeed it can be considered that the network of the $Fe-Cr_2TiO_5$ monoclinic phase grows progressively with the entrance of iron Fe^{3+} (0.785 Å in coordination VI high spin) replacing Cr^{3+} (Shannon-Prewitt ionic radius 0.755 Å in coordination VI). However, the increase in unit cell volume of the $Fe-Cr_2TiO_5$ monoclinic phase due to iron entrance (as the x value diminishes) is reduced by the presence of Cr^{4+} in the structure (replacing Ti^{4+} and acting as reddish chromophore) as it was shown by the UV–Vis–NIR absorption spectra of these samples.

c) For x = 2, the pure Cr_2TiO_5 monoclinic phase is metastable at room temperature and is not synthesized in this study at 1400 °C. Instead, a mixture of Cr_2O_3, $Cr_2Ti_2O_7$, the so-called "E" phase [20] and other unidentified peaks is detected (Fig. 1). In Table 4 and Fig. 6 the values of 33-0409 JCPDS XRD card have been used.

3.5. Effect of mineralizers

As indicated above, in order to study the effect of the presence of flux agents on the reactivity of the system, 10 wt% of several mineralizers were added to the ceramic mixture x = 0.1, which was then fired successively at 1000 and 1100 °C with soaking time of 3 h. The CIE-L*a*b* color parameters of both non-mineralized and mineralized

Table 3
Unit cell parameters of $Fe_2(Cr_xTi_{1-x})O_5$ samples fired at 1400 °C/3 h.

Sample	Crystalline Phase	a (Å)	b (Å)	c (Å)	β(°)	V(Å³)
x = 0	**Pseudobrookite**	9.7958(5)	9.9699(2)	3.72601(3)	-	363.90(1)
x = 0.1	"	9.767(1)	9.9552(3)	3.7354(6)	-	363.22(1)
x = 0.3	"	9.735(1)	9.9133(3)	3.7354(2)	–	360.47(1)
x = 0.5	"	9.712(1)	9.873(2)	3.733(2)	–	357.96(2)
x = 0.5	**Cr_2TiO_5**	7.015(2)	5.001(2)	10.145(4)	110.67(4)	332.96(2)
x = 0.7	"	7.008(3)	5.006(3)	10.102(5)	110.80(2)	331.30(3)
x = 1	"	7.002(2)	4.990(2)	10.064(4)	110.92(4)	328.54(3)
x = 1.5	"	6.974(6)	5.005(2)	10.052(4)	111.25(4)	327.51(4)
x = 2*	"	7.01500	5.01400	9.9370	111.42	325.375

* The values for x = 2 (Cr_2TiO_5), metastable at room temperature and not synthesized in this study, are the values of 33-0409 JCPDS XRD card.
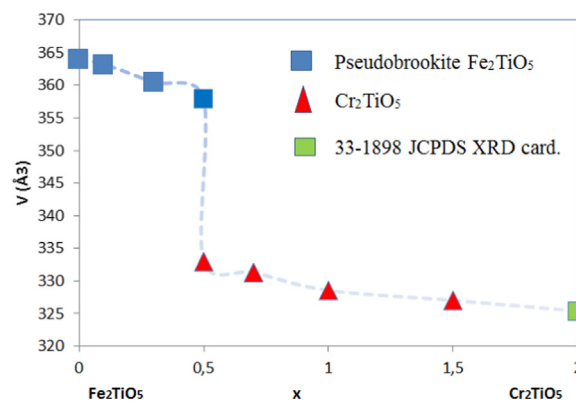
Table 4

CIEL*a*b* of $Fe_2(Cr_xTi_{1-x})O_5$ 5 wt%. glazed samples: x = 0.1, fired at 1000 °C and 10 wt% added mineralizer.

Mineralizer	L*a*b*
Non-mineralized	**43.2/18.8/12.5**
H_3BO_3	46,6/13,9/6,6
NH_4Cl	**42,8/17,2/9,2**
Li_2CO_3	39,8/14,8/6,6
NaF	45,0/9,7/6,3
Non-mineralized and pelleted	45,8/15,0/5,4
NH_4Cl mineralized and pelleted	42,1/15,4/8,1

(10 wt% added mineralizer) samples with x = 0.1 (fired at 1000 °C) and 5 wt%-glazed into the conventional double-firing frit are shown in Table 4. Likewise, several XRD patterns of the sample with x = 0.1 fired at 1000 °C for 3 h are shown in Fig. 7.

According to the data of Table 4, all the mineralized glazed samples, with low temperature (H_3BO_3 and NH_4Cl), middle temperature (Li_2CO_3) and relatively high temperature (NaF) flux agents, show similar L*a*b* values; although the best reddish value (higher a* parameter) is associated with the non-mineralized sample, very similar results are obtained with NH_4Cl addition. On the other hand, both non-mineralized and mineralized samples (x = 0.1) with NH_4Cl were pelleted at 100 bar in a conventional press and fired at 1000 °C for 2 h, in order to analyze the effect of powder compaction (prior to firing treatment) on the reactivity and color of the pigment powders and corresponding glazed samples. The results shown in Table 4 indicate that the compaction pressure does not increase the intensity and reddish shade of glazes.

With regards to powders reactivity, the XRD patterns shown in Fig. 7 indicate that NH_4Cl addition as mineralizer (Fig. 7.c) gives rise to more intense peaks of pseudobrookite than non-mineralized sample (Fig. 7.a). Likewise, compaction pressure also increases the reactivity, both in non-mineralized and in NH_4Cl-mineralized samples, showing the pseudobrookite XRD peaks higher intensity in pelleted samples than its homologous non-pelleted samples. However, as it was previously discussed, the fact of having an increased reactivity, associated with a more advanced crystallization of pseudobrookite, does not involve obtaining better reddish nor more intense colors. The red color is associated with the Cr^{4+} amount into the pseudobrookite lattice rather than with the amount of pseudobrookite crystallization. This behavior is confirmed analyzing the effect of firing temperature on reactivity and the color: despite of the increase of reactivity of the system with temperature, the powders darken and glazed samples show lower reddish shades (high values of L* and low values of both a* and b*) when temperature (reactivity) increases.

3.6. Microstructure analysis

In order to analyze the microstructure of the pigment, some SEM studies were carried out. SEM micrographs of powders with x = 0.1 without mineralizer fired at 1000 and 1200 °C (for 3 h) are shown in Fig. 8. Spheroidal particles of 0.5–2 μm of average particle size are observed at 1000 °C, which increase slightly in size when temperature increases at 1200 °C. On the other hand, the performed SEM-EDX mapping analyses (Fig. 9) show that the Cr distribution in the particles is homogenous, although some segregation of Ti and Fe is observed in agreement with XRD results which show the presence of rutile and hematite as residual crystalline phases.

3.7. Non-conventional methods

The XRD patterns of gel powders (x = 0.1) dried at 110 °C are shown in Fig. 10; nitrates crystallization (such as ammonium nitrate, $(NH_4)NO_3$) is detected in all dried samples, due to the employment of

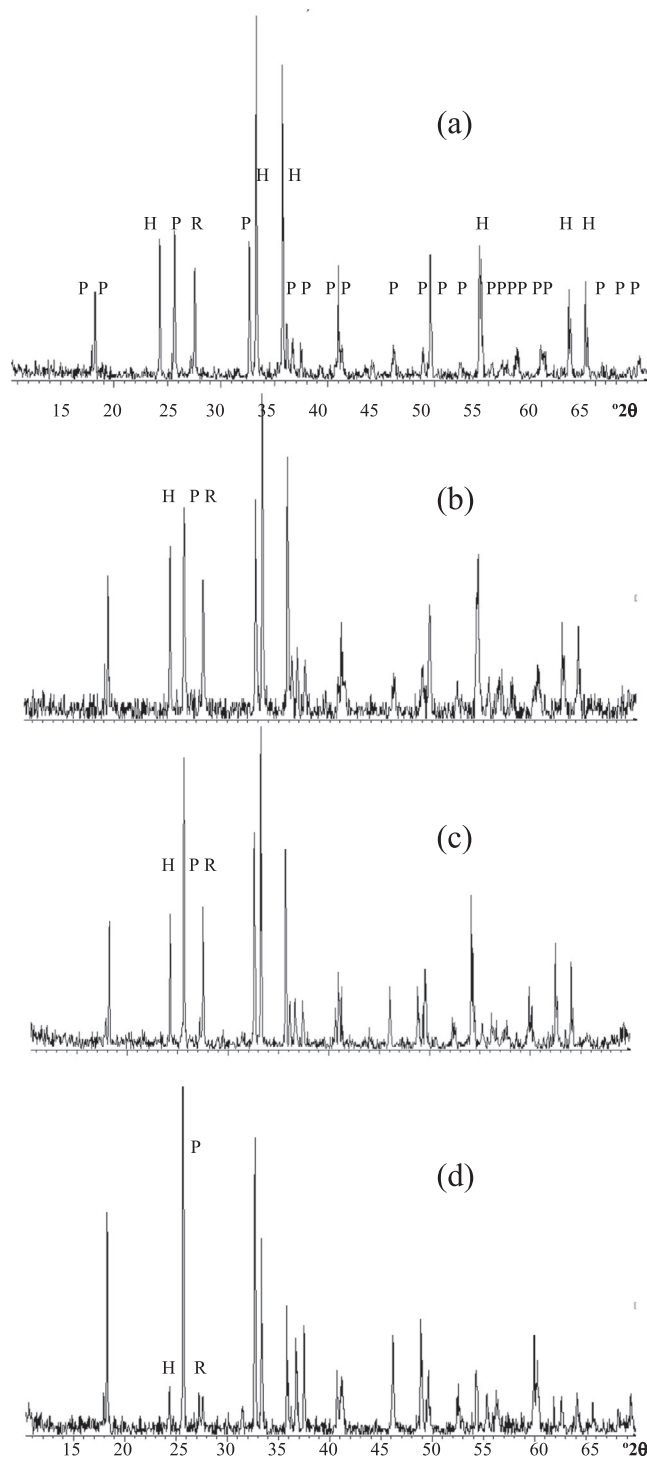**Fig. 7.** XRD of x = 0.1 sample fired at 1000 °C/3 h: (a) non-pelleted, non-mineralized, (b) pelleted, non-mineralized, (c) non-pelleted, NH_4Cl mineralized, (d) pelleted, NH_4Cl mineralized. CRYSTALLINE PHASES: P (Cr-Fe_2TiO_5 pseudobrookite) H (Hematite Fe_2O_3), R (Rutile).

nitrates as precursors, although GP dried gel appears practically amorphous. In the case of gels fired at 500 °C for 1 h, the XRD patterns (not shown) are typical of amorphous samples, due to nitrates decomposition at this temperature. The XRD patterns of gel powders fired at 1000 °C for 3 h are shown in Fig. 11: all fired powders appear more reactive than CE powder, showing low intensity XRD peaks associated with residual hematite and rutile, which are even not detected in CO sample. Similarly to the case of ceramic samples, the increase of
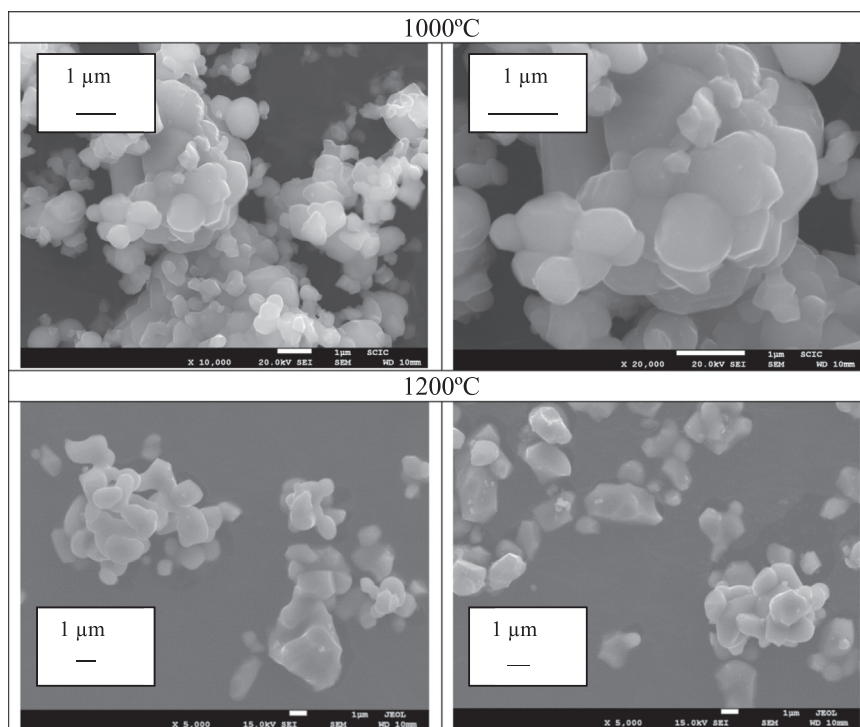
Fig. 8. SEM micrographs of powders with x = 0.1 without mineralizer fired at 1000 °C/3 h and 1200 °C/3 h.
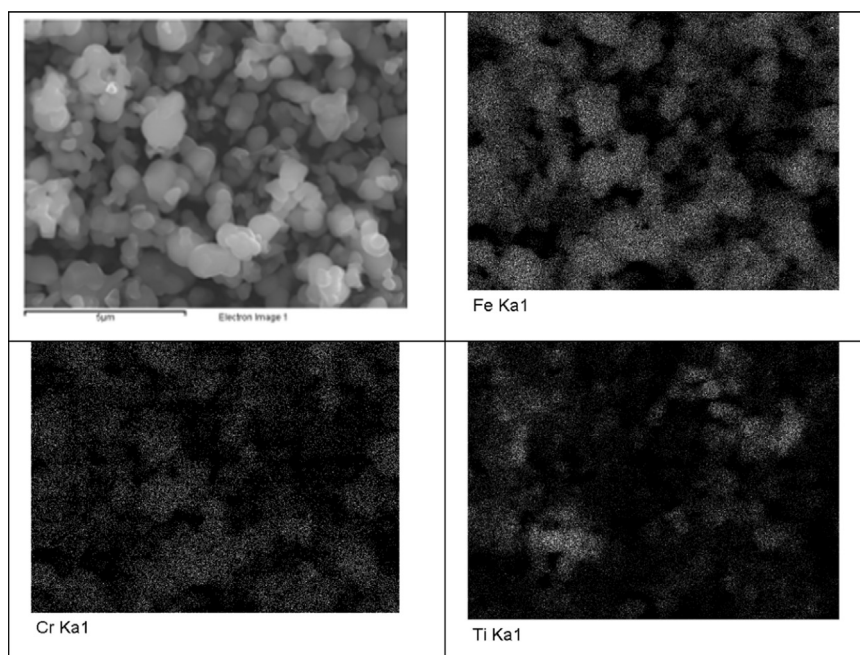

Fig. 9. EDX mapping of powders with x = 0.1 without mineralizer fired at 1000 °C/3 h.

reactivity is not associated with a better red-brown coloring; in effect, the UV–Vis–NIR absorption spectra of gel powders (x = 0.1) fired at 1000 °C, once glazed (5 wt%) within a double-firing frit (Fig. 12), show that the 520 nm band associated with Cr^{4+} in glazed sample exhibits higher intensity for CE sample followed by CO, GP and finally MOD sample. Accordingly, the measured L*a*b* values for these glazed samples (Table 5) indicate that gel samples show a lower red parameter (a*) than CE sample. Finally SEM micrographs of x = 0.1 gel powders fired at 1000 °C for 3 h (Fig. 13) show that the particles conforming the agglomerates are homogeneous and present an average size around 200 nm. The spheroidal particles may be better differentiated in CO

sample; instead, the particles are more heterogeneous in CE sample (Figs. 8 and 9), with particle sizes compressed between 0.5 and 2 μm.

3.8. NIR reflectivity of the optimized pigment

The reflectance values R and R_{NIR} (calculated by Eq. (1) in the range 350–2500 nm or in the range 750–2500 nm, respectively) of the optimized $Cr_{.1}Fe_{1.9}TiO_5$ compared with a commercially available (Zn-Fe-Cr) brown spinel (CPMA 13-37-7) are shown in Table 6: both powder and glazed samples show higher reflectance than the reference brown pigment in all the analyzed wavelenght ranges (total and NIR),
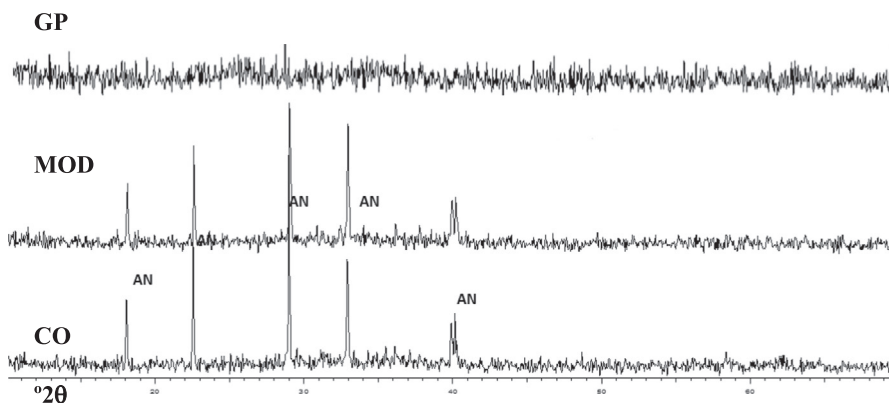
Fig. 10. XRD of non-conventional powders x = 0.1 dried at 110 °C. CRYSTALLINE PHASES: AN (ammonium nitrate $(NH_4)NO_3$). METHODS: CO (coprecipitation), MOD (metal-organic decomposition), GP (polymeric gel)".

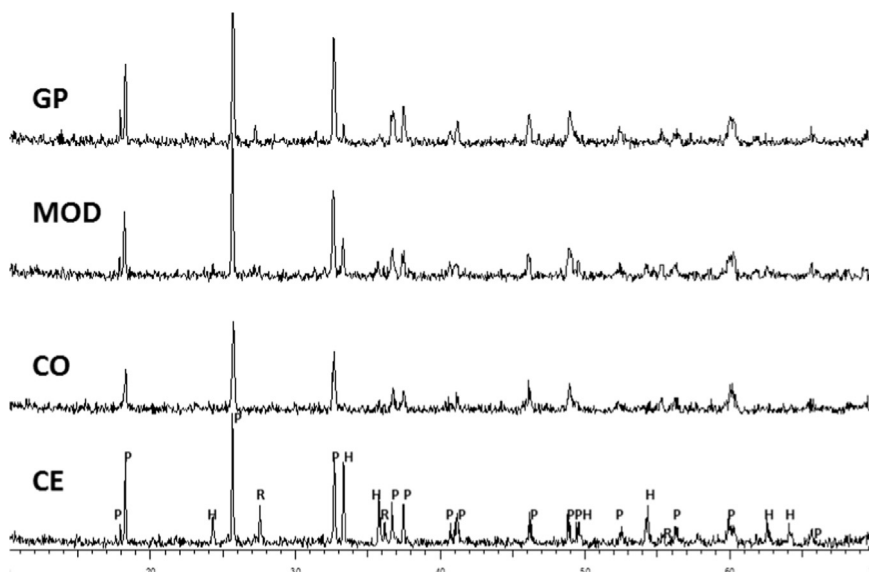**Fig. 11.** XRD of non-conventional powders x = 0.1 fired at 1000 °C/3 h. CRYSTALLINE PHASES: P (Cr-Fe_2TiO_5 pseudobrookite) H (Hematite Fe_2O_3), R (Rutile): METHODS: CE (ceramic), CO (coprecipitation), MOD (metal-organic decomposition), GP (polymeric gel)".
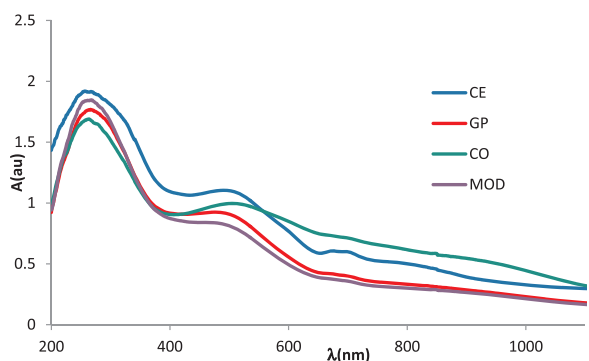

Fig. 12. UV–Vis–NIR absorbance spectra of gel powders x = 0.1 fired at 1000 °C 5 wt% glazed in double firing frit: METHODS: CE (ceramic), CO (coprecipitation), MOD (metal-organic decomposition), GP (polymeric gel)".

indicating the pigment suitability as an energy-saving material (cool pigment). The reflectance spectra in the 350–2500 nm range of the optimized $Cr_1Fe_{1.9}TiO_5$ pigment (both as powder and 5 wt% glazed in double-firing frit) are shown in Fig. 14.

Table 5
CIEL*a*b* of non-conventional samples $Fe_2(Cr_xTi_{1-x})O_5$ x = 0.1 sample, fired at 1000 °C. METHODS: CO (coprecipitation), MOD (metal-organic decomposition), GP (polymeric gel).

	CE	CO	MOD	GP
Dried gels	-	43,5/8,1/8,6	42,4/5,2/6,2	50,7/8,0/13,9
Fired powder	46.2/6.8/7.6	42,4/1,3/0,0	43,0/2,2/0,8	44,0/3,0/1,8
5 wt%. glazed	43.2/18.8/12.5	41,2/16,1/15,6	43,0/5,2/0,8	44,0/6,0/1,8

4. Conclusions

Reddish ceramic pigments based on the solid solution series between Fe_2TiO_5 (orthorhombic pseudobrookite) and Cr_2TiO_5 (monoclinic) have been synthesized and characterized. $Cr_xFe_{2-x}TiO_5$ compositions were prepared by the ceramic route. In order to analyze the pigmenting capacity, the powders were 5 wt% glazed into a conventional double-firing frit (1050 °C). At 1400 °C the reactivity is completed and pseudobrookite crystallizes in the x = 0–0.4 range, both pseudobrookite and monoclinic Fe-Cr_2TiO_5 coexist at x = 0.5, while in the range x = 0.7–1.5 monoclinic Fe-Cr_2TiO_5 crystallizes as the only

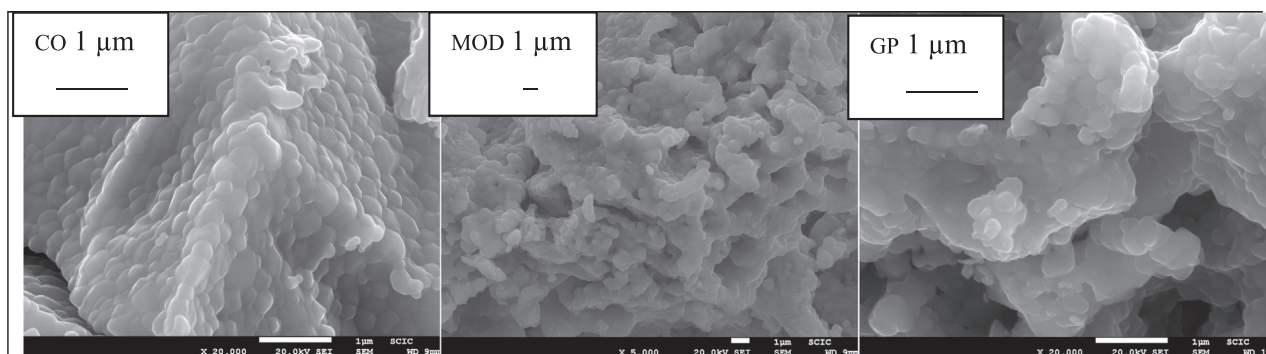**Fig. 13.** SEM micrographs of x = 0.1 gel powders fired at 1000 °C/3 h: METHODS: CO (coprecipitation), MOD (metal-organic decomposition), GP (polymeric gel)".

Table 6
Reflectance measurements in a commercial (Zn-Fe-Cr) brown pigment (CPMA 13–37–7) (M) and the optimized CE x = 0.1 pseudobrookite (P).

	M	M glazed	P	P glazed
R(%) (350–2500 nm)	23	30	35	39
R_{NIR} (%) (750–2500 nm)	33	46	55	54
L*a*b*	42,5/5,2/6,1	32,6/13,0/9,2	46.2/6.8/7.6	43.2/18.8/12.5

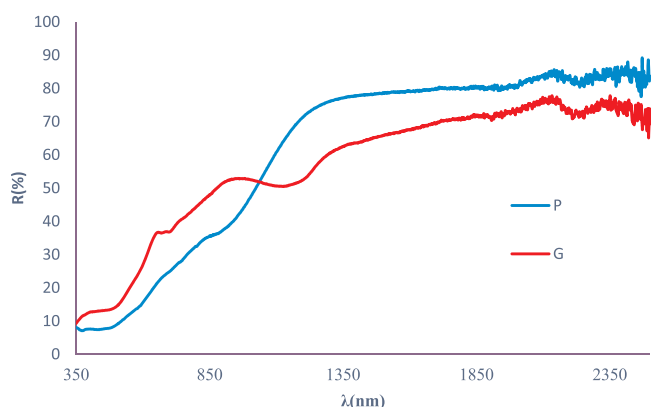**Fig. 14.** Vis-NIR reflectance spectra of optimized CE sample x = 0.1 fired at 1000 °C/3 h: P (powder), G (5 wt% glazed in double firing frit).

crystalline phase; however, this phase is not obtained in x = 2 sample (pure Cr_2TiO_5) in which, even after firing at 1400 °C, only a mixture of Cr_2O_3, $Cr_2Ti_2O_7$, the so-called "E" phase $Cr_2Ti_2O_7$ (along with other unidentified peaks) is detected by XRD. The x = 0.1 sample fired at 1000 °C shows the best red color in the double firing glaze (L*a*b* = 43.2/18.8/12.5), showing pseudobrookite as the main crystalline phase along with residual hematite and rutile detected by XRD.

According with results of UV–Vis–NIR absorption spectroscopy, XRD and CIEL*a*b* measurements, it is observed that the red-brown color of glazed samples is associated to entrance of Cr^{4+} in the lattice and becomes green in unreacted sample x = 2 (showing eskolaite Cr_2O_3 and the so-called "E" phase $Cr_2Ti_2O_7$ as the main crystalline phases). Moreover, the best red-brown colors are not associated to a complete crystallization of pseudobrookite or monoclinic Cr_2TiO_5 phases; indeed, when its crystallization progresses with temperature, powders become practically black colored and glazed samples show poor reddish shades (high L* and low a* and b* values). UV–Vis–NIR absorption spectra of glazed samples show that chromium is the chromophore in the glazes and the valence + 4 dominates, although Cr^{3+} concentration increases when chromium amount increases. This behavior is in agreement with the color and the evolution of the CIEL*a*b* values of glazed samples: the intensity of the color increases always with both chromium amount

and temperature (L* diminishes) and the red-brown chroma tends to blue, due to the enhancement of the 600 nm (orange) absorption band occurring when the chromium amount or temperature increase. The best reddish shade for samples fired at 1400 °C (when the reactivity is completed) is obtained in x = 0.5 sample, since at higher x values (in the monoclinic Fe-Cr_2TiO_5 crystallization field, from x = 0.7 to x = 1.5) the 520 nm band intensity associated to Cr^{4+} in octahedral sites remains stable, indicating a saturation of the chromophore Cr^{4+} concentration.

In the pseudobrookite crystallization field (x = 0 to x = 0.5) the volume of the pseudobrookite unit cell decreases smoothly with the chromium amount according to the entrance of Cr^{4+} (Shannon-Prewitt ionic radius 0.69 Å in coordination VI) in the structure of the pseudo-brookite, replacing Ti^{4+} (0.745 Å in coordination VI). In the Fe-Cr_2TiO_5 monoclinic crystallization field (x = 0.5 to x = 1.5) the volume of the unit cell decreases smoothly with the chromium amount: namely, it grows progressively with the entrance of iron Fe^{3+} (0.785 Å in co-ordination VI high spin) replacing Cr^{3+} (Shannon-Prewitt ionic radius 0.755 Å in coordination VI).

The effect of flux agents analyzed by 10 wt% addition of several mineralizers to the ceramic mixture (x = 0.1) shows that all miner-alized glazed samples present similar L*a*b* values; although the best reddish value (higher a* parameter) corresponds to the non-miner-alized sample, a very similar value is obtained with NH_4Cl addition. On the other hand, both non-mineralized and mineralized (with NH_4Cl) precursor mixtures with x = 0.1 composition were pelleted at 100 bar in a conventional press and fired at 1000 °C for 2 h, showing that the compaction pressure does not increase the intensity (lower L*) and reddish shade (higher a*) of the glazes color. Indeed, although the use of mineralizers and compaction pressure leads to a higher crystal-lization of pseudobrookite with respect to non-mineralized and non-pelleted samples, this is not associated with better reddish colors. Thus, this result confirms that the red color is rather associated with the Cr^{4+} amount into the pseudobrookite lattice and not with the amount of pseudobrookite crystallization.

The preparation of the optimized x = 0.1 sample by non-conven-tional methods, such as coprecipitation (CO), metal-organic decom-position (MOD) and polymeric gel (PG) routes, show that all the fired gel samples appear more reactive than CE powder, showing low in-tensity peaks associated with residual hematite and rutile. However, this reactivity increase is not associated with a better red-brown col-oring, similarly to the results obtained in the studies with mineralizers and pressure. SEM microscopy observations indicate that the gel par-ticles are homogeneous and show an average size around 200 nm; in contrast, the particles are more heterogeneous in CE sample, having a particle size between 0.5 and 2 μm at 1000 °C which increases slightly when temperature increases at 1200 °C. On the other hand, the per-formed SEM-EDX mapping analyses show that the distribution of Cr in the particles is homogenous, although some segregation of Ti and Fe is observed, in agreement with the presence of rutile and hematite as

residual crystalline phases detected by XRD.

The optimized pigment composition $Cr_{.1}Fe_{1.9}TiO_5$ fired at 1000 °C (3 h) show higher NIR reflectance (55% in powder, 54% in glazed sample) than the reference Zn-Fe-Cr brown pigment in all the analyzed wavelenght ranges (total and NIR), indicating the pigment suitability as an energy-saving material (cool pigment).

Acknowledgements

References

[1] L. Pauling, The crystal structure of pseudobrookite, Z. Krist. 73 (1930) 97–112.

[2] G. Monrós, Ronnier Luo (Ed.), Pigment, Ceramic, Encyclopedia of Color Science andTechnology, Springer, 2014(ISBN 978-1-4419-8070-0. ON LINE ISBN 978-3-642-27851-8), ⟨http://www.springerreference.com/docs/html/chapterdbid/348055.html⟩.

[3] J. Rademachers, J.H. Erfurth, F. Hund, Metal additions to pigments of pseudo-brookite-titanium dioxide structure, U.S. patent 4,036,662, 1977.

[4] F. Hund, W. Holznagel, H. Erfuth, F. Kindervater, W. Hennings, U.S. Patent 4,084, 984, 1978.

[5] T.K. atamoto, M. Fujimoto, Heat-resistant yellow pigment with pseudobrookite structure of the formula $Fe_{(2-p-q-r-s)}Li_{(p)}Mg_{(q)}Al_{(r)}Ti_{(s)}O_5$, European Patent 949, 2022, 1999.

[6] T. Suzuki, K. Kataoka, Titanium-iron based composite oxide pigment and method for production thereof, U.S. patent 6,540,824, 2003.

[7] J. Maloney, Titanate pigments: colored rutile, priderite and pseudobrookite structured pigments, in: Edwin B. Faulkner, Russell J. Schwartz (Eds.), High Performance Pigments, Wiley, Freiburg, 2009, pp. 53–76.

[8] M. Dondi, F. Matteucci, G. Cruciani, G. Gasparoto, D.M. Tobaldi, Pseudobrookite ceramic pigments: crystal structural, optical and technological properties, Solid. State Sci. 9 (2007) 362–369.

[9] F. Matteucci, G. Cruciani, M. Dondi, G. Gasparotto, D.M. Tobaldi, Crystal structure, optical properties and coloring performance of karrooite $MgTi_2O_5$ ceramic pigments, J. Solid State Chem. 180 (2007) 3196–3210.

[10] M. Llusar, E. García, M.T. García, C. Gargori, J.A. Badenes, G. Monrós, Synthesis, stability and coloring properties of yellow-orange pigments based on Ni-doped karrooite $(Ni,Mg)Ti_2O_5$, J. Eur. Ceram. Soc. 35 (2015) 357–376.

[11] A. Navrotsky, Thermodinamics of formation of some compounds with the pseudo-brookite structure and of the $FeTi_2O_5$-Ti_3O_5 solid solution series, Am. Mineral. 60 (1975) 249–256.

[12] D. Xirouchakis, A. Smirnov, K. Woody, D.H. Lindsey, D.J. Andersen, Thermodynamics and stability of pseudobrookite-type $MgTi_2O_5$ (karrooite), Am. Mineral. 87 (2002) 658–667.

[13] M. Onoda, Phase transitions of Ti_3O_5, J. Solid State Chem. 136 (1998) 67–73.

[14] I.E. Grey, I. Ward, An X-ray and Mössbauer study of the $FeTi_2O_5$-Ti_3O_5, system, J. Solid State Chem. 7 (1973) 300–307.

[15] A. Navrotsky, Thermodynamics of formation of some compounds with the pseu-dobrookite structure and of the $FeTi_2O_5$-Ti_3O_5 solid solution series, Am. Mineral. 60 (1975) 249–256.

[16] J.F.W. Bowles, Definition and range of composition of naturally occurring minerals with the Pseudobrookite structure, Am. Mineral. 73 (1988) 1377–1383.

[17] F. Ren, S. Ishida, N. Takeuchi, K. Fujiyoshi, Chromium-based ceramic colors, Am. Ceram. Soc. Bull. 71 (1992) 759–764.

[18] G. Seitz, N. Penin, L. Decoux, A. Wattiaux, M. Duttine, M. Gaudon, Near the ferric pseudobrookite composition (Fe_2TiO_5), Inorg. Chem. 55 (2016) 2499–2507, http://dx.doi.org/10.1021/acs.inorgchem.5b02847.

[19] C. Gargori, S. Cerro, N. Fas, M. Llusar, G. Monrós, Red-brown ceramic pigments based on chromium doped ferrian-armalcolite, effect of mineralizers, Ceram. Int. 43 (2017) 5490–5497.

[20] S. Kamiya, S. Hirano, S. Sōmiya, The compound Cr_2TiO_5 in the system $Cr_2O_3.TiO_2$, J. Solid State Chem. 28 (1979) 121–128.

[21] M. Shiojiri, S. Sekimoto, T. Maeda, Y. Ikeda, K. Iwauchi, Crystal structure of Fe_2TiO_5, Phys. Status Solidi 84 (1984) 55–61.

[22] A. Shukla, B.K. Pandey, S.C. Singh, K.N. Uttam, J. Shah, R.K. Kotnala, Alok Kumar, R. Gopal, Liquid-assisted pulsed laser ablation synthesis of titanium ferrite nano-materials, Mater. Focus 4 (2015) 327–332, http://dx.doi.org/10.1166/mat.2015. 1268.

[23] Z.Z. Djuric, O.S. Aleksic, M.V. Nikolic, N. Nikolic, G.B. Brankovic, P.M. Nikolic, Structural, morphological and optical study of nanostructured TiO_2/Fe_2O_3 thick film, in: Proceedings of the 45th International October Conference on Mining and Metallurgy, Bor Lake, Bor, Serbia,16–19 October 2013.

[24] D. Hanžel, F. Sevšek, Characterization of monoclinic Fe_2TiO_5 by Mössbauer spectroscopy and magnetic susceptibility, Mat. Res. Bull. 19 (1984) 35–43.

[25] W.Q. Guo, S. Malus, D.H. Ryan, A. Altounian, Crystal structure and cation distributions in the $FeTi_2O_5$-Fe_2TiO_5 solid solution series, J. Phys. Condens. Matter 11 (1999) 6337–6346.

[26] T. Armbruster, E.V. Galuskin, L.Z. Reznitsky, E.V. Sklyarov, X-ray structural investigation of the oxyvanite (V_3O_5) – berdesinskiite (V_2TiO_5) series: V^{4+} substituting for octahedrally coordinated Ti^{4+}, Eur. J. Mineral. 21 (2009) 885–891.

[27] CPMA Classification and chemical description of the complex inorganic color pigments, fourth ed. Alexandria, Dry Color Manufaturers Association, 4 th. ed, 2013.

[28] POWCAL and LSQC programmes, Dpt. Of Chemistry, University of Aberdeen,UK.

[29] Harry G. Hecht, The interpretation of diffuse reflectance spectra, J. Res. Natl. Bur. Stand.-A. Phys. Chem. 80A (4) (1976) 567–583.

[30] G. Kortüm, Reflectance Spectroscopy, Principles, Methods, Applications (ISBN 978-3-642-88071), Springer, 1969.

[31] CIE Comission International de l'Eclairage, Recommendations on Uniform Color Spaces, Color Difference Equations, Psychometrics Color Terms. Suplement n°2 of CIE Pub. N°15 (E1-1.31), Bureau Central de la CIE, Paris, 1971, p. 1978.

[32] Standard solar irradiation, American Society for Testing and Materials(ASTM) Standard G173-03 ⟨http://rredc.nrel.gov/solar/spectra/am1.5/⟩.

[33] S. Sōmiya, S. Hirano, S. Kamiya, Phase relations of the Cr_2O_3-TiO_2 system, J. Solid State Chem. 25 (1978) 273–284.

[34] A. García, M. Llusar, J. Badenes, M.A. Tena, G. Monrós, Encapsulation of hematite in zircon by microemulsion and Sol-Gel methods, J. Sol.-Gel Sci. Technol. 27 (2003) 267–276.

[35] S.W. Karickhoff, G.W. Bailey, Optical absorption spectra of clay minerals, Clays Clay Miner. 21 (1973) 59–70.

[36] M. Dondi, F. Matteucci, G. Cruciani, G. Gasparoto, D.M. Tobaldi, Pseudobrookite ceramic pigments: crystal structural, optical and technological properties, Solid. State Sci. 9 (2007) 362–369.

[37] H. Eilers, U. Hömmerich, S.M. Jacobsen, W.M. Yen, K.R. Hoffman, W. Jia, Spectroscopy and dynamics of Cr^{4+}:$Y_3Al_5O_{12}$, Phys. Rev. B Condens. Matter 49 (22) (1994) 505–513.

[38] G. Monrós, H. Pinto, J. Badenes, M. Llusar, M.A. Tena, Chromium(IV) stabilisation in new ceramic matrices by coprecipitation method: application as ceramic pigments, Z. Anorg. Allg. Chem. 631 (2005) 2131–2135.

[39] S.R. Prim, A. García, R. Galindo, S. Cerro, M. Llusar, M.V. Folgueras, G. Monrós, Pink ceramic pigment based on chromium doped $M(Al_{2-x}Cr_x)O_4$, M = Mg, Zn, normal spinel, Ceram. Int. 39 (2013) 6981–6989.

[40] F. Matteucci, C. Lepri Neto, M. Dondi, G. Cruciani, G. Baldi, A.O. Boschi, Color development of red perovskite pigment $Y(Al,Cr)O_3$ in various ceramic applications, Adv. Appl. Ceram. 105 (2006) 99–106.

[41] R.D. Shannon, Revised effective ionic radii and systematic studies of interatomic distances in halides and chalcogenides, Acta Cryst. A32 (1976) 751–767.